DESIGN AND MAGNETIC MEASUREMENT RESULTS OF THE HALF STORAGE RING MAGNETS*

T. H. Sun, H.-L. Xu†, B. Liu, G. Feng
University of Science and Technology of China, Hefei, China

Abstract

The Hefei Advanced Light Facility (HALF) is a fourth generation synchrotron light source under construction, centered on a 2.2 GeV diffraction limited storage ring (DLSR) with a design natural emittance below 85 pm·rad. The storage ring has a circumference of nearly 480 m and contains 880 magnets in 20 lattice cells, including longitudinal gradient bends (LGB), reverse bends (RB), quadrupoles (Q), sextupoles (S), octupoles (O), and all corrector magnets (CR). As of early 2026, all magnet types except the octupoles had completed series production and factory magnetic measurements. This paper presents the physical design methodology and key magnetic measurement results of the HALF storage ring magnets, and also outlines ongoing studies on Preisach hysteresis modeling and on magnetic crosstalk in selected compact magnet assemblies through three dimensional simulations and stretched wire measurements.

INTRODUCTION

HALF adopts a compact hybrid multi-bend achromat lattice to achieve ultralow emittance within a limited circumference [1], as shown in Fig. 1. The densely packed layout gives short magnetic lengths, while the 13 mm good field region and field-quality target of $< 0.05\%$ require relatively large apertures [2]. The resulting small aspect ratios strengthen fringe fields and make magnetic crosstalk between adjacent magnets non-negligible.

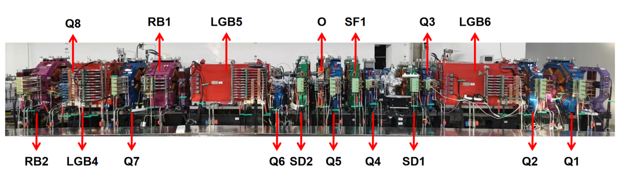

Figure 1: The lower half-cell of the HALF storage ring mockup, showing the compact arrangement of the main magnets. Corrector magnets are omitted for clarity.

To address these constraints, a Gauss–Newton algorithm (GNA) and Non-dominated Sorting Genetic Algorithm II (NSGA-II) workflow was used to design the HALF storage ring multipole magnets [2]. Within the good field region, the optimized multipole components were controlled to the 10^{-4} level, and magnetic measurements show that all magnets satisfy the physics requirements over their specified tuning ranges.

The closed orbit of the storage ring is jointly provided by the longitudinal gradient bends and the reverse bends. By longitudinally redistributing the bending field, longitudinal gradient bends can suppress quantum excitation and reduce the beam equilibrium emittance. To accommodate a future energy upgrade of HALF to 2.5 GeV, an electromagnetic variable-gap concept was adopted for these magnets, offering more accurate and reproducible field tuning over a wide operating range than permanent magnets commonly used in fourth generation light sources [3]. Using a design code based on the actual beam trajectory, all 123 longitudinal gradient bends in the storage ring, including three prototypes, have been fabricated and measured. The results confirm that the field homogeneity, trajectory control, and series consistency satisfy the design requirements.

The latter part of this paper also briefly discusses ongoing studies, including further investigations of magnetic crosstalk and hysteresis effects in magnets.

DESIGN AND MEASUREMENT RESULTS FOR HALF MAGNETS

Multipole Magnets

The GNA/NSGA-II workflow in Fig. 2 was implemented in MATLAB and coupled with OPERA for field evaluation [4, 5]. GNA was used for relatively simple objectives, whereas NSGA-II was used for more stringent field-quality optimization. To remain consistent with rotation coil measurements, the objective function was defined from weighted multipole components normalized to the main field. For a quadrupole magnet, it is written as

$$F_Q = \sum_{m=1}^{4} W_m \, b_{2(2m+1)}^2, \qquad m = 1, 2, 3, 4.$$

In the geometric model, the initial pole shape was placed symmetrically on the positive semiaxis of the Y axis, and the profile perturbation was parameterized using a Legendre series to preserve contour smoothness and suppress local-

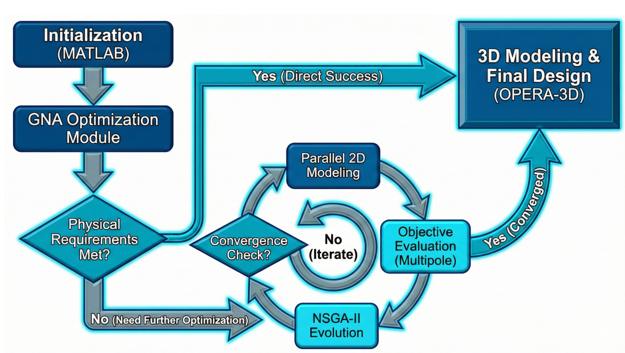

Figure 2: Optimization workflow for the multipole magnets.

* This Work is supported by the National Nature Science Foundation of China under Grant No. 12075239.
† hlxu@ustc.edu.cn

saturation effects. The perturbation was applied only to the Y coordinate:

$$yvar_k = \sum_{l=1}^{L} \beta_l \, P_l\left(2 \times \frac{k-1}{K-1} - 1\right)$$

Here, P_l denotes the Legendre polynomial, L is the highest order, β_l is the relative coefficient, k is the index of the discrete contour point along the pole profile, and K is the total number of contour points included in the optimization [6].

Magnetic measurements were carried out using Hall probe and rotation coil methods. Except for the octupoles, all storage ring magnets have completed series production and passed factory magnetic acceptance measurements. The rotation coil measurements covered excitation curves, normalized multipole components, and magnetic center offsets. For the quadrupole and combined-function dipole-quadrupole magnets, the physics requirements at the good-field region are $B_3/B_2 \le 0.05\%$, $B_4/B_2 \le 0.05\%$, $B_5/B_2 \le 0.03\%$, and $B_6/B_2 \le 0.015\%$.

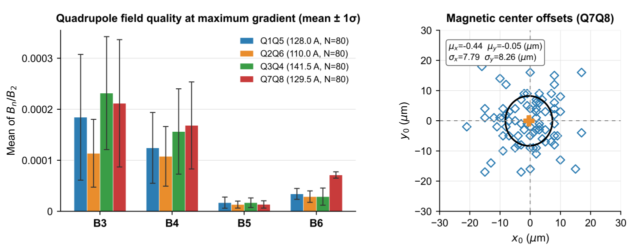

Figure 3: Multipole components of the quadrupoles at maximum gradient and the magnetic center offsets of Q7/Q8.

Table 1: Summary of field quality in reverse bends and sextupoles at maximum operating strength.

(a) Reverse bends: RB1 (100.8 A) and RB2 (96.6 A)

Order	Mean (RB1)	Std. Dev. (RB1)	Mean (RB2)	Std. Dev. (RB2)
B3	2.829×10^{-4}	1.238×10^{-4}	2.074×10^{-4}	9.771×10^{-5}
B4	1.018×10^{-4}	5.892×10^{-5}	6.857×10^{-5}	4.936×10^{-5}
B5	2.130×10^{-5}	1.431×10^{-5}	3.140×10^{-5}	5.451×10^{-6}
B6	8.293×10^{-6}	5.700×10^{-6}	1.235×10^{-5}	3.806×10^{-6}

(b) Sextupoles: SF1/SD2 (84.96 A) and SD1 (82.55 A)

Order	Mean (SF1/SD2)	Std. Dev. (SF1/SD2)	Mean (SD1)	Std. Dev. (SD1)
B4	3.657×10^{-4}	2.065×10^{-4}	3.431×10^{-4}	2.048×10^{-4}
B5	2.283×10^{-4}	1.320×10^{-4}	1.728×10^{-4}	1.004×10^{-4}
B6	5.532×10^{-5}	3.695×10^{-5}	5.143×10^{-5}	2.323×10^{-5}
B9	3.608×10^{-5}	2.017×10^{-5}	4.776×10^{-5}	2.022×10^{-5}

Figure 3 summarizes the quadrupole multipole components at maximum gradient and the magnetic center offsets of Q7/Q8. The quadrupole field quality generally satisfies the design requirements. The nominal Q7/Q8 gradients lie entirely within the linear excitation region, whereas the maximum gradient in Fig. 3 is the upper tuning limit with more than 10% strength margin after the planned 2.5 GeV upgrade. The largest magnetic-center shift, close to 12 µm, occurs only near this high-gradient saturation region and is acceptable for the specified operating range. Table 1 summarizes the rotation coil results for the reverse bends and sextupoles at maximum operating strength. For the sextupoles, the correction coils introduce extra multipole components and slightly attenuate the main field; at the maximum correction strength, the main sextupole field decreases by about 1%, and the difference between correction paths is about 0.1%.

Longitudinal Gradient Bending Magnets

All longitudinal gradient bends use an electromagnetic variable-gap scheme to meet the field-tuning requirements for the planned upgrade from 2.2 GeV to 2.5 GeV. Because the peak field will reach approximately 1 T after the upgrade, a tapered pole-root expansion is used to mitigate local saturation. Each magnet has a main coil and one auxiliary coil placed on the highest-field pole, and the pole gap is adjusted to improve agreement between the measured and ideal field profiles (Fig. 4). With a pole-gap machining tolerance of ±0.02 mm and a vertical assembly error of ±0.03 mm, the measured-to-ideal profile deviation remains below 0.3%. Measurements at the 2.5 GeV setting showed almost unchanged integrated-field homogeneity relative to 2.2 GeV, although the LGB1 and LGB3 auxiliary-coil currents required an adjustment of about 0.1% to compensate for partial pole saturation. A scheme based only on pole-gap adjustment would require much larger gaps at low-field poles, increasing end fringe fields and making it unsuitable for the compact HALF layout.

With appropriate pole shape shimming and end chamfering, the longitudinal gradient bends achieved good field quality within the good field region. Based on Hall probe measurements on different vertical planes, the longitudinal integrated field homogeneity (see Fig. 5), the integrated field homogeneity along the actual trajectory, and the trajectory deviation were evaluated. The results show that the deviation of the actual trajectory from the ideal trajectory remains below 40 µm at all longitudinal positions. For batch-produced magnets, integral long coil measurements were used as the primary method for factory tests of field homogeneity and excitation curves, while Hall probe measurements served only as a supplementary tool for characterizing the longitudinal field distribution.

ONGOING STUDIES

Crosstalk Calculation and Measurement

The compact magnet layout in the HALF storage ring reduces the minimum spacing between adjacent main magnets to only 49 mm, making magnetic crosstalk unavoidable in practice. Crosstalk was analyzed using OPERA TOSCA

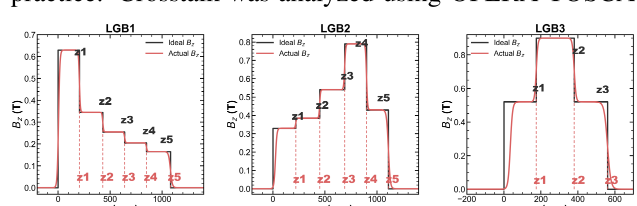

Figure 4: Longitudinal distributions of the vertical magnetic field for the three types of longitudinal gradient bends.

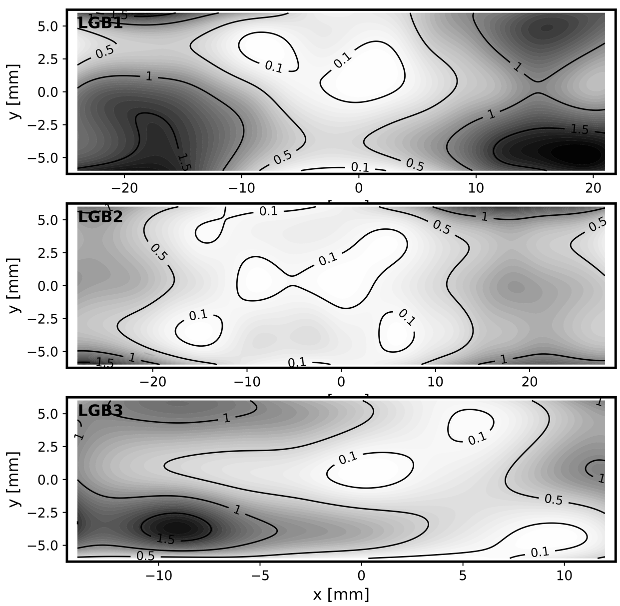

Figure 5: Contour maps of the longitudinal integrated field homogeneity for the prototypes of the three longitudinal gradient bends. The contour values are given in units of 10^{-4}.

after convergence tests. Here, we present only the representative Q4-SF1 case, which has been numerically analyzed and experimentally validated. To clarify the dependence of crosstalk on the magnet operating point, the Q4-SF1 combination was calculated under several current combinations. The results show that the crosstalk effect decreases as the magnetic saturation of the two magnets increases. Over the calculated current range, the maximum reduction in the integrated gradient of Q4 is about 0.06%; at the maximum-gradient setting, this reduction decreases to about 0.023%.

To validate the calculation, integrated field measurements of Q4 before and after the installation of SF1 were carried out using a stretched wire bench. After the installation of SF1, the simulated reduction in the integrated gradient of Q4 is about 0.06%, while the measured value is about 0.074%. The deviation among three repeated measurements is below 0.01%, and the difference between simulation and measurement is below 0.02%.

The crosstalk associated with the main bending magnets was also evaluated. Among the storage ring magnets, the most pronounced case occurs for LGB3, which is affected simultaneously by the two adjacent quadrupoles Q7 and Q8. The combined crosstalk from these quadrupoles reduces the maximum bending angle of LGB3 by about 0.14%. This effect is small but not negligible for orbit control, and will therefore be compensated by adjusting the LGB coil current during magnet setting and storage ring commissioning.

Hysteresis Effect

During storage ring commissioning, magnet operating points often move between the ascending and descending branches of the excitation loop. Because of hysteresis, the field produced by a magnet depends on both the instantaneous current and the excitation history [7, 8].

Using multi-path rotation coil data, we constructed a Preisach hysteresis model for the Q7/Q8 quadrupoles. The training set consists of two major loops of 0 A–150 A–0 A with current steps of 15 A and 7.5 A, and the prediction set is taken from a minor loop within 75 A ± 15 A. Because the HALF quadrupoles show weak hysteresis, narrow loops, and some saturation at high excitation, a seventh-order polynomial fitted to the midline of the ascending and descending branches of the major loop was used as the baseline, and the model was trained on the residual after baseline removal and normalization. Combined with two-stage optimization and smoothness constraints, the model shows improved stability and minor loop prediction capability. As shown in Fig. 6, the current implementation reproduces the overall trend of the minor loop, although further improvement in prediction accuracy is still needed.

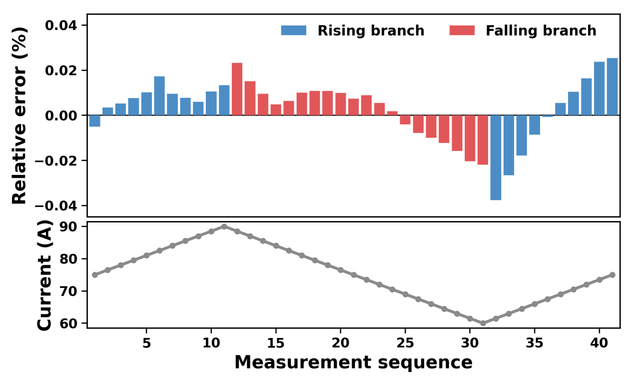

Figure 6: Relative prediction error of the minor loop and the corresponding excitation sequence. The upper panel shows the relative prediction error as a function of measurement sequence, and the lower panel shows the corresponding excitation current sequence.

CONCLUSION

In summary, this work has completed the physical design and magnetic measurements of the main magnets in the HALF storage ring. Except for the octupoles, all other magnet types have completed series production and factory magnetic measurements, and their overall performance satisfies the physics requirements. The longitudinal gradient bends meet the design targets in integrated field homogeneity, trajectory deviation, and series consistency. Numerical analysis and stretched wire measurements of magnetic crosstalk under the compact layout show good agreement, confirming the reliability of the evaluation method. Initial progress has also been achieved in Preisach hysteresis modeling for commissioning applications.

REFERENCES

[1] Z. Bai *et al.*, "A modified hybrid 6ba lattice for the half storage ring", in *Proc. IPAC'21, Campinas, Brazil*, pp. 407–409, 2021. doi:10.18429/JACoW-IPAC2021-MOPAB112

[2] T. Sun *et al.*, "Status of multipole magnets for hefei advanced light facility", *IEEE Transactions on Applied Superconductivity*, vol. 34, no. 5, pp. 1–6, 2024. doi:10.1109/TASC.2024.3355366

[3] T. Sun, X. Huang, Z. Zhang, B. Liu, Z. Ren, and H. Xu, "Status of longitudinal gradient bending magnets for hefei advanced light facility", *Journal of Instrumentation*, vol. 20, no. 04, P04028, 2025. doi:10.1088/1748-0221/20/04/P04028

[4] The MathWorks, Inc., MATLAB version: 24.2 (r2024b), 2024, https://www.mathworks.com

[5] Dassault Systèmes, SIMULIA Opera, Dassault Systèmes, 2025, https://www.3ds.com/products/simulia/opera

[6] Gël. Le Bec, J. Chavanne, P. N'gotta, *et al.*, "Shape optimization for the esrf ii magnets", in *Proc. IPAC'14, Dresden, Germany*, pp. 1232–1234, 2014. doi:10.18429/JACoW-IPAC2014-TUPRO082

[7] K.-H. Hoffmann and Günter. H. Meyer, "A least squares method for finding the preisach hysteresis operator from measurements", *Numerische Mathematik*, vol. 55, no. 6, pp. 695–710, 1989. doi:10.1007/BF01389337

[8] R. Roussel *et al.*, "Differentiable preisach modeling for characterization and optimization of particle accelerator systems with hysteresis", *Physical Review Letters*, vol. 128, no. 20, p. 204801, 2022. doi:10.1103/PhysRevLett.128.204801